On the reliable measurement of specific absorption rates and intrinsic loss parameters in magnetic hyperthermia materials

R R Wildeboer[1], P Southern[2] and Q A Pankhurst[3]

[1] MIRA Institute for Biomedical Engineering and Technical Medicine, University of Twente, Enschede, the Netherlands
[2] Resonant Circuits Limited, c/o UCL Healthcare Biomagnetics Laboratory, 21 Albemarle Street, London W1S 4BS, United Kingdom
[3] UCL Institute of Biomedical Engineering, University College London, Gower Street, London WC1E 6BT, United Kingdom

E-mail: q.pankhurst@ucl.ac.uk

Abstract

In the clinical application of magnetic hyperthermia, the heat generated by magnetic nanoparticles in an alternating magnetic field is used as a cancer treatment. The heating ability of the particles is quantified by the specific absorption rate (SAR), an extrinsic parameter based on the clinical response characteristic of power delivered per unit mass, and by the intrinsic loss parameter (ILP), an intrinsic parameter based on the heating capacity of the material. Even though both the SAR and ILP are widely used as comparative design parameters, they are almost always measured in non-adiabatic systems that make accurate measurements difficult. We present here the results of a systematic review of measurement methods for both SAR and ILP, leading to recommendations for a standardised, simple and reliable method for measurements using non-adiabatic systems. In a representative survey of 50 retrieved datasets taken from published papers, the derived SAR or ILP was found to be more than 5% overestimated in 24% of cases and more than 5% underestimated in 52% of cases.

Keywords: magnetic hyperthermia, specific absorption rate, intrinsic loss parameter

(Some figures may appear in colour only in the online journal)

1. Introduction

Magnetic hyperthermia is an emerging medical technology designed to destroy malignant cancers by using magnetic nanoparticles (MNPs) that produce heat in response to the application of an external alternating magnetic field (AMF) [1–4]. If proven clinically, it has the potential to become an extremely versatile and valuable focal therapy, since in principle the heat will only be produced in the local environment of the MNPs. This means that if the particles are confined to the region of the cancerous tumour tissue, the surrounding healthy tissue will be left unharmed [5].

The principle of magnetic hyperthermia has been known for more than 50 years, with the first publication by Gilchrist *et al* in 1957 [6]. However, over the last decade interest has been dramatically fuelled by the achievements of Jordan *et al* in bringing the technology into clinical trials for brain cancer and prostate cancer [7, 8]. In 2013 alone, 682 publications appeared in scientific and clinical literature on the topic of magnetic hyperthermia [9]. Many of these papers contain reports on new synthetic routes or processing methods to achieve MNPs with better or improved magnetic heating characteristics.

This search for MNPs with optimal heating characteristics is motivated by the basic clinical imperative that the

hyperthermia technology should be safe and well tolerated by patients, while also being an effective cancer treatment. In particular, the AMF itself must be safe and well tolerated. In clinical terms, this means that the magnetic field strength and/or frequency must be low enough to avoid the induction of tissue-borne eddy currents strong enough to generate harmful levels of non-specific heating and/or unacceptably high levels of peripheral nerve stimulation [10, 11]. Thus, if a particle can be found which has the same heating characteristics as another, but with a lower requirement regarding field strength or frequency, it is clinically preferred.

Moreover, it may be difficult to deliver therapeutically sufficient concentrations of MNPs to a tumour site, especially in cases where direct injection of the particles into the tumour is not an option. In such cases, it is important that the MNPs display the best possible heating properties and generate as much heat as possible for a given AMF strength and frequency.

For these reasons, it is important to be able to make a physically robust and reliable assessment of the magnetic heating properties of any given MNP in its clinically useful state, i.e. in the form of a fluid suspension, as would be used for interstitial injection. A critical factor here and one that is not always taken into account, is that most measurements are performed under non-adiabatic experimental conditions. It is also important to be able to directly compare the results reported by different research teams, even when they are using substantially different measurement apparatus and experimental conditions.

Unfortunately, it is clear from inspection of the current scientific literature that neither of these conditions is being met and there is a chronic need for a more standardised approach. We hope here to contribute to meeting this need by reporting on a detailed assessment of the best available means for measuring the magnetic heating properties of MNPs and the preferred ways of reporting and comparing these.

2. Parameters for reporting magnetic heating properties

The most commonly quoted measure for magnetic heating ability of MNPs is the specific absorption rate (SAR), which is defined as the heating power (P, measured in W) generated per unit mass (m_{MNP}, measured in g):

$$SAR = P / m_{MNP}. \qquad (1)$$

It may be argued that this definition of the SAR parameter can lead to confusion, especially in the clinical community where the SAR terminology is ingrained but has a rather different meaning. Clinically, SAR is used to denote the transfer of energy into the human body by radio frequency electromagnetic fields, such as that generated by mobile phone use or exposure to MRI scanners, and also by other means, such as ultrasound. In the clinical context, the SAR refers to the power dissipation per gram of living human tissue.

In the magnetic hyperthermia definition of SAR, the mass is that of the magnetic material alone. Although it can be said that the expected amount of heat transfer into human tissue should be small in comparison to that delivered to the MNPs, this does express an assumption that peripheral heating effects,

such as eddy currents, are negligible. Furthermore, the SAR parameter as reported in the vast majority of magnetic hyperthermia papers is determined by suspending the MNPs in an *in vitro* tissue analogue, which is almost always water. As such, the SAR values reported do not reflect the situation one might expect to find in human tissue, where heat dissipation by physiological means, such as increased blood flow, is to be expected.

Perhaps in recognition of this inherent difficulty with nomenclature, some authors refer to the parameter defined in (1) as the specific loss power (SLP), specific power loss (SPL) or specific heat power (SHP). However, it has been suggested that a distinctly different, more intrinsic parameter should be used for the special case of magnetic hyperthermia.

The power produced by any given MNP is determined by the physical and magnetic properties of that MNP, which is manifest in the imaginary part of its magnetic susceptibility χ'' [12]. However, the power also scales linearly with the frequency (f, measured in Hz) and quadratically with the strength of the AMF (H, measured in A m^{-1}). Removing these extrinsic factors, one arrives at the intrinsic loss power (ILP, measured in Hm^2 g^{-1} [1, 13]):

$$ILP = SAR / fH^2. \qquad (2)$$

which, in the rather more convenient units of nano–Henrys m^2 per kg, computes as:

$$ILP\ [nHm^2kg^{-1}] = \frac{SAR\ [W\,kg^{-1}]}{f\,[kHz]\ \ H^2\,[(kAm^{-1})^2\,]}. \qquad (3)$$

It should be noted that, due to the field and frequency dependence of χ'', the ILP parameter can only be considered constant in relatively low field strength and low frequency regimes [5]. However, as these same conditions apply to the requirements for clinically acceptable limits in the AMF field and frequency, this is not a significant limitation for the comparison of materials intended for use in clinical magnetic hyperthermia.

In the remainder of this paper, we will refer to both the SAR and ILP parameters as defined in equations (1) and (2); however, it is our recommendation that the ILP parameter be used in preference to SAR when reporting the specific case of magnetic hyperthermia heating from ensembles of magnetic nanoparticles.

3. Measurements under non-adiabatic conditions

Both the SAR and the ILP parameters are essentially measures of power dissipation, and as such they are determined by calorimetric measurements that are best performed under adiabatic conditions in which there is very limited external heat transfer. However, such adiabatic measurement systems are difficult to build [13, 14] and the measurements themselves are time-consuming [15]. Consequently, adiabatic systems are seldom used, and almost all reported work on magnetic hyperthermia is performed on non-adiabatic apparatus.

While using non-adiabatic systems is in itself not problematic, neglecting or failing to take into account the attendant heat losses can be, and can result in the SAR/ILP values being underestimated–as shown by the comparison of SAR/
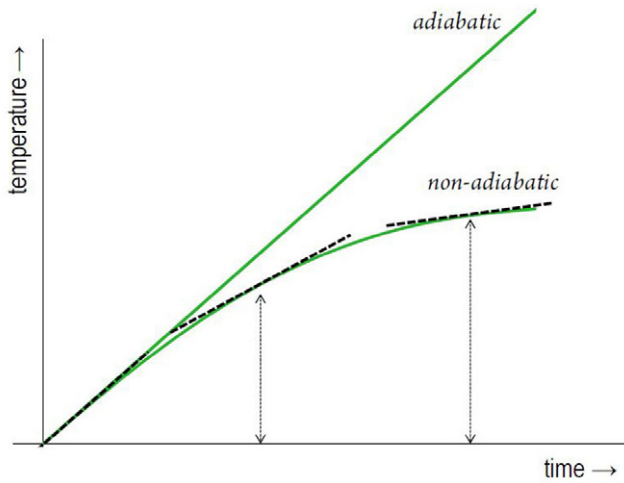
J. Phys. D: Appl. Phys. **47** (2014) 495003

R R Wildeboer *et al*

Figure 1. Typical heating curves obtained in calorimetric measurements with an adiabatic and a non-adiabatic setup.

ILP values determined on identical samples using different calorimetric setups [14–16]. In one example, Natividad *et al* found the non-adiabatic SAR value to be 21% lower than the adiabatic value [17]. Non-adiabaticity might also help explain a reported discrepancy between theoretical and experimental SARs, a factor two times difference for calculations using an experimental χ'' and even more for those using a χ'' found by Debye approximation [18].

Despite this potential problem, non-adiabatic systems can be used for quick and reliable SAR/ILP measurements, without the need for an extensive, time-consuming and expensive adiabatic setup. Using the experimental and analytical methods described below, we believe that accurate calorimetric measurements can be made, as long as the losses from the non-adiabatic setup are quantified and included in the calculation of results.

4. Theoretical background to SAR and ILP measurements

An adiabatic setup does not allow heat transfer between the MNP sample and its surroundings. Consequently, all heat produced by the MNPs is invested in the temperature rise of the sample. In this ideal case, the sample's temperature is only dependent on the power P deposited by the MNPs and the heat capacity of the sample (C, measured in $J\,K^{-1}$):

$$C \cdot \frac{dT(t)}{dt} = P. \qquad (4)$$

A measurement of the temperature rise during the application of an AMF will therefore yield a linear heating curve, as shown schematically in figure 1.

In non-adiabatic setups, however, the sample starts losing heat energy to the environment as soon as its temperature is higher than that of the space or materials surrounding it (T_0). There are several mechanisms of this heat loss:

- Conduction involves the heat transfer from the medium to adjoining materials and scales with the temperature difference $T - T_0$, surface area and thermal properties [19, 20].

- Convection, heat transfer by movement or diffusion of a heated medium, takes place in the air around the sample [19]. Usually one discriminates natural convection, movement that is solely caused by the temperature gradient, from forced convection which involves cooling by already-moving air [20].
- In the higher temperature difference ranges radiation becomes more dominant, when it increases with $T^4 - T_0^4$ [15, 19, 21].
- Eventually, the sample will also start losing energy due to evaporation or melting of the sample. This strongly non-linear energy loss appears when the temperature near the heat source approaches the boiling or melting point of one of the sample's substances, even when the average temperature of the sample is well below that point. As these phase transitions cause cooling [19], the concentration changes and the thermal properties of another phase might be different, which can strongly influence the heating curve [22].

All these heat loss mechanisms cause the heating trend to curve downwards as the temperature increases (see figure 1).

In most studies in which the heating curve is used to estimate the power generated by MNPs, the heat loss is assumed to be linearly dependent on the difference in temperature between the sample and its surroundings. The temperature rise can then be elegantly described by the following differential equation [14]:

$$C \cdot \frac{d\Delta T(t)}{dt} = P - L \cdot \Delta T. \qquad (5)$$

Here, L (measured in $W\,K^{-1}$) is a constant that quantifies the proportionality between the temperature and the losses and ΔT is the difference in temperature ($T - T_0$). This means that the slope of the heating curve decreases with the temperature of the sample until the lost energy per unit time is equal to the input, and the temperature saturates at a steady state. The solution to this differential equation is expressed by [14, 21]:

$$T - T_0 = \frac{P}{L}\left(1 - e^{-\frac{t - t_0}{C/L}}\right). \qquad (6)$$

In the magnetic hyperthermia literature, this phenomenological equation is commonly referred to as the Box–Lucas equation [13, 23–25].

It should be noted that the linear-loss assumption is a relatively demanding one, and that it only holds for low temperature differences. If one takes into account all possible losses, the relation between temperature and losses becomes non-linear, especially for higher temperatures. A more comprehensive description of the heating curve would be:

$$C \cdot \frac{dT(t)}{dt} = P - P_L(T). \qquad (7)$$

In this, $P_L(T)$ is a non-linear function that describes the power loss for each temperature. The presence of radiation and its fourth-power temperature dependence suggests that one would need at least a fourth-order polynomial to approach this function. In practice, as described in section 5.1, it is found that this is a good approximation.

For these equations to be valid, however, there is also another demanding assumption to be made, namely that the T or ΔT that is measured should represent the temperature or change in temperature experienced by the entire sample. However, this is seldom the case, as even though the temperature is generally considered homogeneously distributed [14], it is governed by diffusion and convection within the sample and is therefore non-uniform [26, 27]. This leads to both temporal and spatial effects. Regarding temporal effects, discussion in the literature has focused on the time taken for heat to spread within the sample, compared to the time for the heat to spread to the surroundings [28], with some stating that the internal heat flow should be at least 10 times faster than that to the surroundings [14]. In practice, however, such effects are seldom encountered in magnetic hyperthermia experiments where the time constant of the thermal probe measurement is in the order of seconds–and indeed, we saw no evidence of them in our observations. Spatial effects are, however, much more pronounced, and in particular the location of the thermal probe within the sample is important (see section 5.3).

There are other aspects that may also contribute to the accuracy of the measurement:

- Delayed heating causes inaccuracy as it takes some time for the heat curve to take off after the heating has started [15]. When this delay is not taken into account, a linear fit from $t = 0$ underestimates the slope and the heating is perceived to be lower than it actually is. This is discussed in section 5.4.
- Temperature-dependence of the heat capacity might influence the heating behaviour in different temperature regimes [16]. The total heat capacity is the weighted average of all substances in the measurement container $C = \sum c_i \cdot m_i$ [14]. The heat capacity of water, however, scarcely changes in the relevant temperature range (<1%). Moreover, the heat capacity might include an unknown part of the container that also heats up during AMF application and confounds the results. In practice however, we find that these possible heat capacity related effects do not appear to be significant factors (see section 5.5).
- Magnetic field inhomogeneities may have a considerable effect on the total heat generated, especially since–at least under clinically applicable conditions–the SAR scales with the square of the field [26]. The solution to this is to ensure that the coil design used delivers as homogeneous a field as possible, e.g. by using a solenoid or Helmholtz configuration for the coils. Good homogeneity has also been reported from electromagnetic circuits [29].
- Inherent losses in the heating system must be considered, since no system has 100% efficiency and there are losses in any system where an electrical signal is translated into a magnetic field. Also, external sources can alter the calorimetric behaviour, since they can unintentionally heat up as well as cool down the sample. Both of these effects can lead to what we term 'peripheral heating', which is best determined experimentally on a system-by-system basis (see section 5.2).
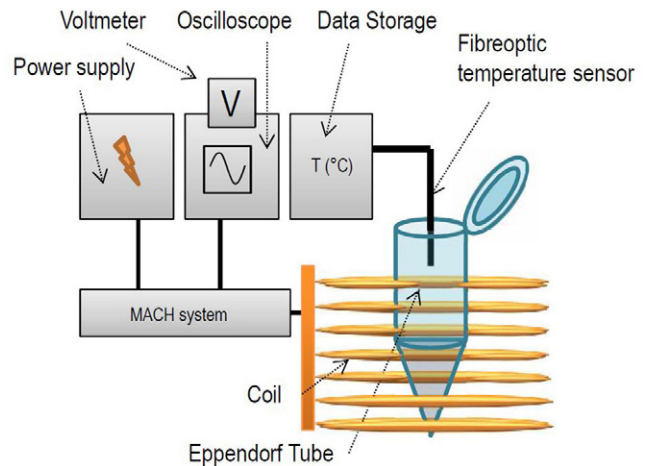

Figure 2. Schematic illustration of the experimental setup used in this work. Radio frequency AMF was supplied using a Magnetic AC Hyperthermia (MACH) system made by Resonant Circuits Ltd (London).

We will not go into particle-specific variations of the heating ability due to temperature or higher magnetic field strengths, since those inaccuracies are not caused by the setup but by the particles themselves.

5. Measuring SAR/ILP: experimental considerations

Experiments were performed in a custom-made setup that comprised a parafilm-covered plastic Eppendorf tube or glass vial containing the MNP sample, fibre-optic temperature measurement probes (Luxtron FOT Lab Kit, accuracy 0.2 °C, sample frequency 1 Hz), and a water-cooled solenoid magnetic coil attached to a Magnetic AC Hyperthermia (MACH) system made by Resonant Circuits Ltd. Figure 2 shows a schematic drawing of the setup used, which conforms to published descriptions of 'a typical experimental setup' [14]. Indeed, many groups working on SAR/ILP measurements report similar non-adiabatic systems in their publications (e.g [18, 22, 24, 26, 30–49].).

Some groups surround their samples with holders of varying insulating strengths, such as Styrofoam or other thermally insulating materials, while others do not [27]. We have chosen here to use no superficial insulation.

Experiments were performed using two commercially available magnetic nanoparticle suspensions. One was Ferucarbotran (Meito Sangyo Corp, Osaka), a biocompatible superparamagnetic iron oxide nanoparticle [50, 51] that has been used in several previous studies [52, 53]. The other was the 50 nm MNP fluid, FluidMAG-UC/A (Chemicell GmbH).

5.1. Linear loss regime

The degree of loss linearity was investigated in three different samples, comprising 1.0 ml, 0.5 ml and 0.25 ml respectively of Ferucarbotran at a concentration of 14 mg of iron per ml, measured under identical conditions. Each sample was heated to 75 °C, whereupon a cooling curve was obtained, i.e. the temperature T was recorded as a function of time t. The numerical derivatives of the cooling curves were then computed,
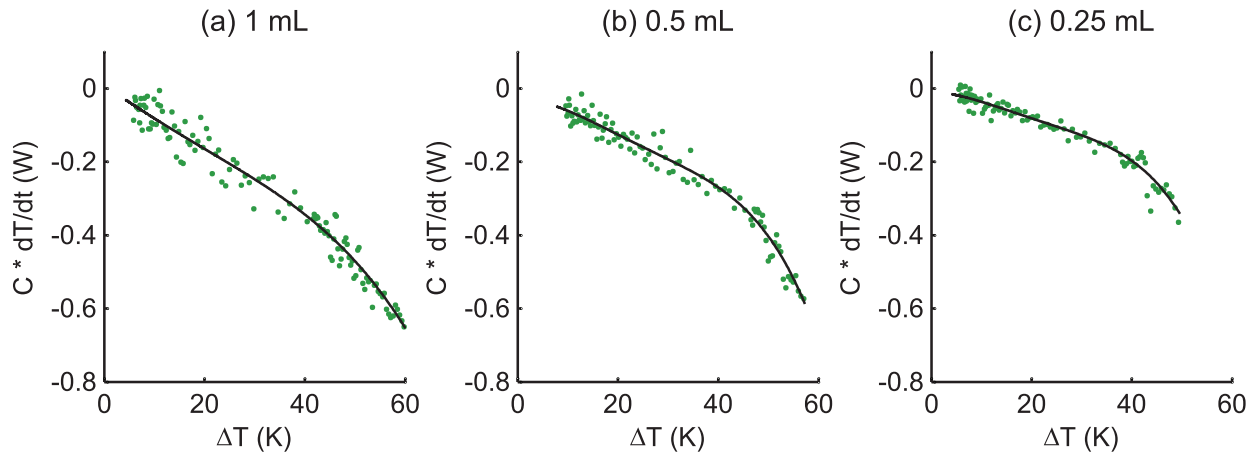
Figure 3. The numerical derivatives of a cooling curve versus the temperature difference after heating of a (*a*) 1 ml, (*b*) 0.5 ml and (*c*) 0.25 ml sample of a commercial ferrofluid, Ferucarbotran (Meito Sangyo Corp, Osaka). Fourth order polynomial fits are displayed in black lines, deviating from linear trends displayed as dotted lines; datapoints were recorded every second and the numerical derivatives were calculated as the moving average of three consecutive datapoints.

assuming a heat capacity for the system of $C = C_V \cdot V$, where $C_V = 4.18 \, \mathrm{J\,K^{-1}\,ml^{-1}}$ and V is the volume in ml. These were then plotted as $C(dT/dt)$ against the temperature difference $\Delta T = T_{\max} - T(t)$, as shown in figure 3.

For the 0.5 ml sample, a linear loss is observed for ΔT values up to 35 °C, with a slope of ca. 6.7 mW K^{-1}. The losses increase non-linearly for higher temperatures. Following the previously mentioned hypothesis for $P_L(T)$ (in equation (7)), we expect that the losses might follow a non-linear relationship that is at least proportional to the temperature difference to the power four. Therefore, polynomial fits of the fourth order are also shown. On the face of it, these expressions describe the losses fairly well.

Since changing the sample volume changes the ratio of the sample volume to its surface area, it is to be expected that the behaviour of the losses would also change. This was clearly observed, as shown in figure 3, where the linear loss regime for the 1.0 ml sample was larger, at ca. 40 °C and for the 0.25 ml sample was smaller, at ca. 30 °C. The rates of loss were also different, being higher for the 1.0 ml sample, at ca. 8.5 mW K^{-1} and lower in the 0.25 ml sample, at ca. 4.2 mW K^{-1}. This hierarchy is to be expected given that the larger the volume, the more heat there is to be dissipated for each degree K in cooling; but the shape effects are apparent in that the rates of loss do not simply scale with sample volume.

It is clear therefore that both the extent of the linear loss regime and the rate of loss within that regime are setup-dependent parameters that should be expected to vary between different measurement systems, and even for a given system, will also vary as a function of sample volume and morphology. Nevertheless, it is also clear that the linear loss approximation embodied in equation (5) is an attainable experimental condition, so that reliable measurements of both SAR and ILP should be readily achievable.

5.2. Peripheral heating

To assess the extent to which there might be a peripheral heating effect on water-borne MNP dispersions placed within

the magnetic heating apparatus, a pure water sample of 0.5 ml, containing no magnetic particles at all, was brought into the setup. The water temperature was measured for a period of 25 min during the application of an AMF of different field amplitudes (5–14 kA m^{-1}), corresponding to different currents (see figure 4). Significant heat rises of 1 °C or more were seen for all but the smallest AMF.

The origin of this peripheral heating effect is not precisely known, but it is likely to be a combination of an induced eddy current effect in the polar fluid and a radiative heating effect from the AMF system itself. It is therefore likely also to be an effect that will vary from system to system in different laboratories. In our laboratory setup, we conducted some exploratory tests (not shown) on both pure water and a salt solution at physiological concentrations, which indicated that after 10 min of heating the temperature difference between the two was no more than 0.1 K. Given that the induced eddy current effect should be strongly dependent on the electrical conductivity of the sample, we infer that at least in our setup, the peripheral heating effect is dominated by radiated heat from the apparatus itself. In any case, from the observations in figure 4 one can conclude that peripheral heating can be a significant factor in the measured heating curves, and that, in particular, the initial heating slope may be affected. This is significant as the initial slope is often used as the key determinant of the SAR/ILP measurement (see below).

Various strategies may be adopted to minimise the influence of the peripheral heating effect. We explored the possibility of using a water-only heating curve as a calibration curve, measured immediately before the sample of interest and then subtracted from the obtained $T(t)$ curve. However, in practice this leads to delays and uncertainties as one needs to allow the heating apparatus to return to the same initial state before each measurement. A better and more elegant solution would be to measure both the water and the sample simultaneously and record the difference between the temperatures of the two [29]. However, this requires that the heating apparatus be able to accommodate the water and the sample under identical conditions, which in many cases (including ours) is not feasible. For
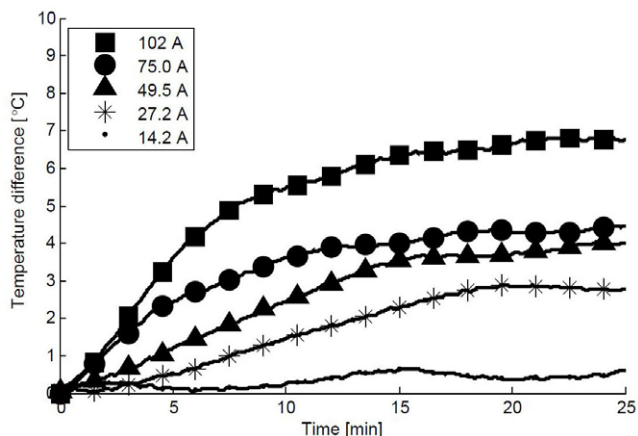
J. Phys. D: Appl. Phys. 47 (2014) 495003

R R Wildeboer *et al*

Figure 4. Heating of a 0.5 ml water sample under application of alternating currents of amplitudes ranging from 14.2 to 102 A through a water-cooled, seven-ringed solenoid coil. The temperature differences are measured relative to room temperature (22 °C).

this reason, we have adopted a third approach which is to allow the system to 'warm up' (i.e. equilibrate) to the temperature it will reach when the specific field is applied (i.e. the baseline), before starting a measurement. This procedure was adopted for all subsequent measurements reported below.

5.3. Temperature distribution

An inhomogeneous spatial distribution of temperature is to be expected in any sample that is heated in a non-adiabatic system. The causes for this include steady-state diffusion and convection effects, as well as the inhomogeneous dissipation of heat from the sample into its environment, either from its surface or through the walls of the sample container.

These temperature distributions may be significant, as illustrated in the thermal camera images shown in figure 5 for the case of two commonly used sample holders–a plastic Eppendorf tube with a tapered bottom section and a glass flat-bottomed cylindrical vial. It is clear therefore that the location of the thermal probe within the sample is an important factor to consider when measuring the temperature of the sample. Indeed, it has been suggested that the most accurate measurements are carried out just beneath the sample surface [26]; however, since the temperature is the highest at that location, the average temperature rise of the entire sample might be overestimated.

To further investigate the temperature distributions in the samples, heating curves were recorded from identical 0.5 ml volume samples of Ferucarbotran (diluted in water to 7 mg ml^{-1} of iron oxide) using multiple fluoroptic probes placed at different locations in the sample holders (see figure 6).

Two configurations were examined: one corresponding to the differences in temperature vertically, on the cylindrical axis of the holders, between the top and bottom of the fluid; and one radially, at the top of the fluid, just below the meniscus, between the centre and the edge of the sample (see figure 7). The data show that, in the 25 to 65 °C range in which most SAR/ILP measurements are made, differences of 1–2 °C appear in both
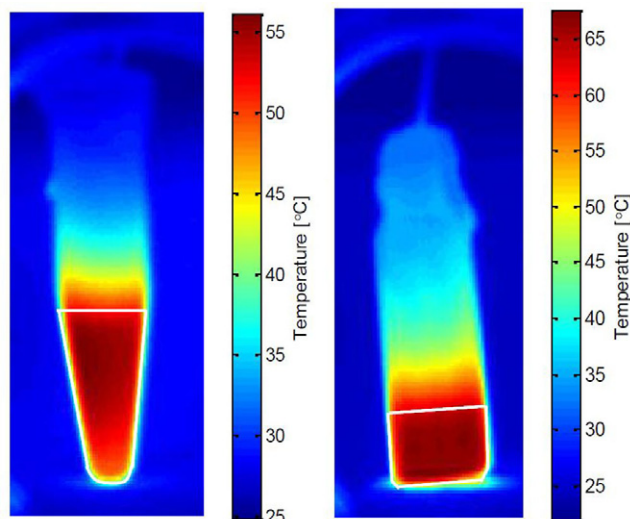

Figure 5. Thermal images of an Eppendorf tube and a glass vial, after magnetic heating. The white lines show the location of the 0.5 ml samples held within the respective containers.
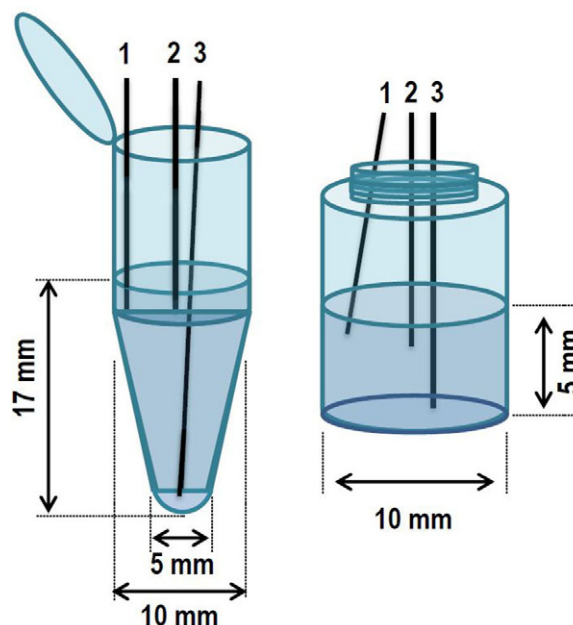

Figure 6. Dimensions and probe positions of the conical-tipped plastic Eppendorf tube and flat-bottomed glass vial used as sample holders.

containers for radial displacement of the fluoroptic probe and in the glass vial for vertical displacement. Larger temperature differences of up to 7.5 °C were measured between the top and the bottom of the fluid in the Eppendorf tube.

These results show that in the case of the flat-bottomed vial, any probe that is positioned more or less centrally within the fluid will record a local temperature that is representative (within ± 1 °C) of the mean temperature of the entire volume. However, in the case of the conical Eppendorf holder, significant differences in the recorded temperature may appear, dependent on the probe position. If this is not appropriately accounted for, inaccurate or misleading results might be obtained.
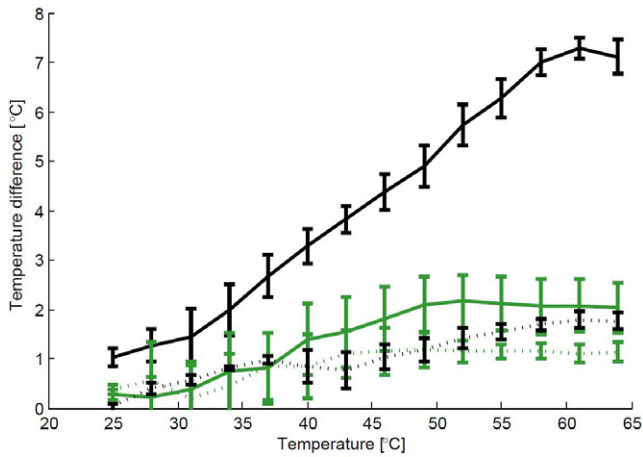
J. Phys. D: Appl. Phys. 47 (2014) 495003

R R Wildeboer *et al*

Figure 7. The mean difference in temperature, averaged over six consecutive heating curves, recorded by two separate fluoroptic probes placed at different locations in the same 0.5 ml Ferucarbotran sample, in either a cylindrical glass vial (green symbols) or a plastic Eppendorf tube (black symbols). The dashed lines refer to the differences between the temperatures recorded by probes at locations 1 and 2 in figure 6, $\Delta T = T_2 - T_1$, plotted as a function of T_2. The solid lines refer to the differences between probes at locations 2 and 3, $\Delta T = T_2 - T_3$, plotted as a function of T_2. The error bars show the standard deviations of the means.
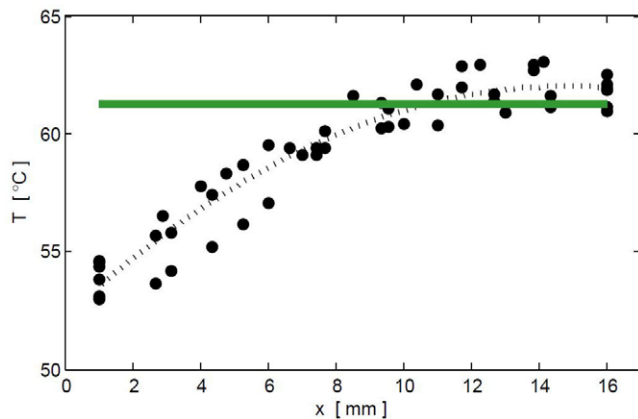

Figure 8. The temperature distribution in a standard Eppendorf tube of a magnetically heated 0.5 ml Ferucarbotran sample, as a function of distance along the central axis from the bottom (x = 0 mm) to the top (x = 17 mm). The green line represents the overall average temperature of the fluid, calculated from the geometrical shape of the Eppendorf and the temperature trend represented by the dotted black line.

For this reason, we examined further the local temperatures $T(x)$ recorded by the fluoroptic probe as a function of its displacement x along the central axis of the Eppendorf tube (see figure 8). The sample was heated and held in steady state by balancing the AMF-supplied magnetic heating to the ambient thermal losses to the environment. $T(x)$ was found to vary smoothly from ca. 54 °C at the bottom of the tube, to ca. 62 °C at the top of the tube.

The mean temperature of the entire 0.5 ml sample was then estimated numerically as $T_{\mathrm{mean}} = \sum_i T(x_i) \cdot V(x_i) / \sum_i V(x_i)$, where $V(x_i)$ is the volume of a horizontal slice of the container
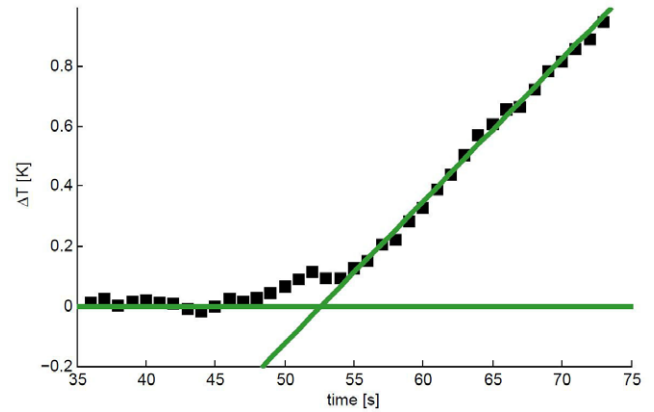

Figure 9. Typical example of time delay in a heating curve, plotted as a function of time near the moment (at $t = 47$s) that the AMF was switched on. The superimposed straight lines are linear fits to the first few and the last few data points in this interval.

at position x_i. This calculation gave $T_{\mathrm{mean}} \approx 61$ °C, corresponding to the temperature measured at $x \approx 10$ mm, a point ca. one-third of the distance from the meniscus of the liquid sample to the bottom of the Eppendorf tube.

In light of these findings, we recommend the use of two temperature probes at different locations in the sample as a way of both monitoring and correcting for the non-uniform temperature distribution. In the case of the 0.5 ml sample in an Eppendorf tube, we find that the mean of the temperatures recorded from fluoroptic probes positioned just underneath the meniscus and two-thirds of the way towards the bottom of the tube, represents the average temperature very well. Alternatively, one probe placed at one-third distance below the sample's surface can be used. In the case of an 0.5 ml sample in a cylindrical flat-bottomed container, the temperature distribution is almost homogeneous, so that a centrally placed probe or pair of probes gives a good measure of the average temperature.

5.4. Delayed heating

Temporal effects are to be expected at the outset of any experiment. In the case of magnetic heating, there may be many causes, including the time constant associated with the inductive heating mechanism, the time associated with the establishment of any diffusion or convection within the fluid and the intrinsic response time of the temperature probes.

We have observed such effects in our system, as illustrated in figure 9, which shows a typical instance in which a time delay of ca. 5s was measured between the time that the MACH heating system was switched on and the time that an observable thermal response was recorded.

Delayed heating is not necessarily a confounding factor in the measurement of heating effects, so long as it is known and accounted for. However, as discussed in section 6.1, there are some analytical approaches to computing SAR/ILP that rely on estimating the initial slope of the heating curve, in which case the possibility of incorrect measurement becomes more likely.

5.5. Total heat capacity

Lastly, we consider which heat capacity value should be used in the SAR/ILP calculations. In the literature, it is often assumed (either explicitly or implicitly) that the heat capacity of a sample equals the heat capacity of an equivalent volume of pure water. However, this neglects any possible contribution to the heat capacity from the sample holder or the sample environment.

To test whether the contributions of the container to the heat capacity are indeed negligible, the ILP values of an 0.5 ml (20 mg ml^{-1} iron oxide) FluidMAG UC/A sample were obtained from a sample in a flat-bottomed glass vial, and from the same sample in a geometrically identical, 3D-printed poly(lactic acid) (PLA) vial. The glass vial was of mass 2.4 g and heat capacity 1.70 J K^{-1}, while the PLA was lighter, at 1.4 g and had a higher heat capacity of 2.35 J K^{-1} [54].

To test the hypothesis that the only heat capacity that need be considered is that of the suspension medium, i.e. water, the ILP vales were calculated assuming that to be the case. In three separate measurements in each vial, ILP values of 1.68 ± 0.10 nHm^{2}kg^{-1} and 1.66 ± 0.03 nHm^{2}kg^{-1} were measured for glass and plastic, respectively, under application of a 3.8 kA m^{-1} and 989 kHz AMF. Given that the differences between the values obtained in the two containers are well within their respective standard deviations, it appears that the assumption is indeed valid.

6. Measuring SAR/ILP: analytical models

We turn our attention now to the analytical models and methods used to extract the SAR and/or ILP parameters from magnetic heating (and cooling) measurements. We have identified five such distinguishable methods, some of which are simple but prone to error, and others that are reliable but, as yet, seldom used by practitioners. Given the importance attached to getting this analytical aspect of the SAR/ILP determination right, we will describe and discuss each method in turn, then provide a comparative test to establish which are best suited to general use.

6.1. Initial slope method

In this most commonly used method, one tries to approximate the slope of the initial heat rise, β [15]. The underlying assumption is that the initial slope of the curve does not suffer from losses since the sample is at its baseline temperature:

$$\beta = \frac{dT}{dt}\Big|_{t\to0} = \frac{d}{dt}\left(\frac{P}{C}\left(1 - e^{-\frac{t}{L/C}}\right)\right)\Big|_{t\to0} = \frac{P}{C}. \quad (8)$$

Therefore, the SAR can be computed using:

$$\text{SAR}_{\text{Initial-slope}} = \beta C / m_{\text{MNP}}. \quad (9)$$

However, since heat transfer mechanisms may already be significant at the onset of the heating curve, e.g. because the temperature of the sample may already be above the baseline temperature, this method might be sensitive to inaccuracies [15]. Also, as seen in section 5.4, delayed heating effects might complicate the initial slope measurement.

Furthermore, as Andreu and Natividad (2013) found in their review, even within this method, there are several different computation methods that have been applied [14]. Expanding on their overview of the literature, in a representative random survey we found seven groups with a linear fit to the first tens of seconds of the heating curve [17, 42, 55–59], the intervals ranging from 10 to 100s [27]; three groups with an extrapolated polynomial fit [60–62]; nine groups directly calculating the slope from the ΔT and Δt in a particluar interval [26, 32, 36, 38, 41, 44, 63–65]; and nine groups taking a numerical derivative of the entire $\Delta T(t)$ curve, of which three used the constant slope [25, 34, 43] and six the maximum slope [21, 30, 35, 66–68] to calculate β. This variety of approaches is likely to result in a variety of results.

To explore this further, we recorded the first 30s (taking account of the delayed heating effect) of a typical magnetic heating curve and made five different linear approximations to its slope (see figure 10). These were: the linear part of a polynomial fit to the curve; a 'direct' estimate $(\Delta T(t = 30\,s) - \Delta T(t = 0)\,)/\Delta t$ where $\Delta t = 30\,s$; the maximum and median slopes calculated numerically in 3s rolling intervals over the range; and a simple linear fit to the full dataset. Three of these methods yielded similar values and on inspection appear to accurately reflect the actual slope of the curve, but the linear part of the polynomial fit gave a 20% larger value and the maximum numerical derivative estimate was 60% larger. We conclude that the latter two methods are not appropriate for use in this way.

6.2. Decay method

This relatively uncommon method uses the steady state temperature $T_{\text{ss}} = P / L$ as well as the characteristic time of the system cooling down ($\tau = C / L$) to determine SAR [14, 21]:

$$\text{SAR}_{\text{Decay}} = (T_{\text{ss}} / \tau)\,(C / m_{\text{MNP}}). \quad (10)$$

As with the initial slope method, uncertainty in the decay method arises from the many ways to determine τ, either by fitting or using numerical derivatives. Moreover, it is not always verifiable whether the steady state temperature has been reached in a reasonable amount of time–and even if it has, the system must be in the domain for which linear loss can be assumed, and $T_{\text{ss}} = P / L$ holds.

6.3. Corrected slope method

This new method, derived by the authors, corrects the value determined by the (initial) slope method for any linear losses already apparent at that temperature ($P = C\,(dT / dt) + L\Delta T$). When the value of thermal loss L of the system is known, one can calculate the SAR using:

$$\text{SAR}_{\text{Corrected-slope}} = \left(C\frac{dT}{dt} + L\Delta T\right)/m_{\text{MNP}}. \quad (11)$$

In this equation ΔT is the (mean) temperature difference between the sample and baseline, which, of course, must be within the bounds of the linear-loss regime. Even when the loss L is not known, it is possible to calculate its most
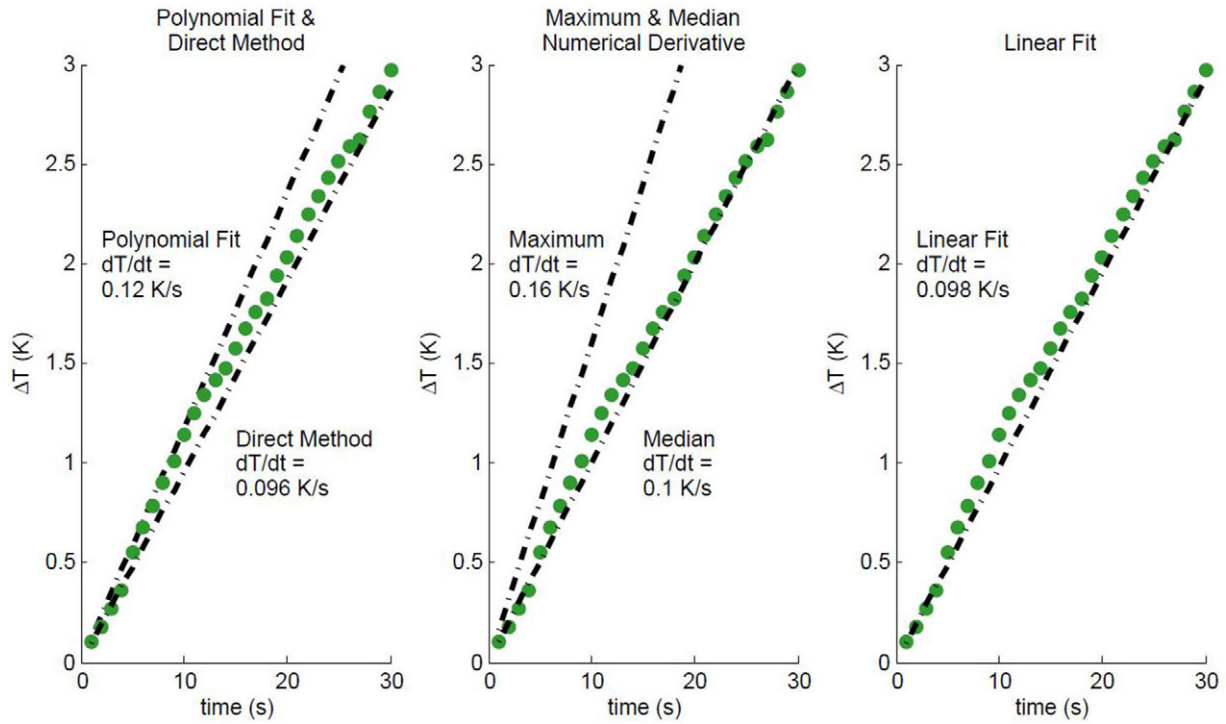
Figure 10. Comparison of five different linear approximations to the initial slope of the same set of magnetic heating data, $\Delta(t)$, recorded from $t = 0$ to $t = 30$ s, as described in the text.

probable value by determining the slope for multiple temperatures along the heating curves (appendix 1).

6.4. Box–Lucas method

As described in equation (7), in the linear-loss regime the heating curve should follow a Box–Lucas equation. Therefore, a least-squares fit to the following expression can be used [13, 21, 24, 25]:

$$\Delta T = A \left(1 - \exp\left(-\lambda \left(t + t_0 \right) \right) \right). \tag{12}$$

One can then use the fitting parameters A and λ to compute the SAR, since $A\lambda = T_{ss}\tau^{-1} = P/C$:

$$\text{SAR}_{\text{Box-Lucas}} = A\lambda C / m_{\text{MNP}}. \tag{13}$$

The t_0 parameter, correcting for a non-zero start of the curve, is generally not needed or used.

6.5. Steady state method

Lastly, one can wait for the system to reach the steady state temperature and calculate the losses that are associated with that temperature. Since the input power equals the dissipated losses in the steady state condition ($T_{ss} = P / L$), the SAR is then:

$$\text{SAR}_{\text{Steady-state}} = T_{ss} L / m_{\text{MNP}}. \tag{14}$$

In this method, the loss parameter L has to be determined. This can be done using the corrected slope method described above or through an experiment similar to that presented in figure 3.

7. Discussion

Even after taking into account all of the experimental considerations in section 5, it is apparent that the determination of the SAR or ILP value is dependent on the choice of analytical method in section 6. This was clearly seen in the ILP determinations using the initial slope method in figure 10, where in an extreme case the slope was overestimated by 60%.

To assess the relative accuracy of the different methods, we have tested them against a calibration standard based on the heating of a 10 ml water sample using an immersed 56 Ω electrical resistor. A current of 90 mA was passed through the resistor, delivering P = 0.45 W of power. The $\Delta T(t)$ curve was recorded and then analysed as if it were a magnetic heating curve. The resulting 'SAR'/P values thus obtained are shown in figure 11, where it is clear that of the five methods, only the corrected slope and the Box–Lucas fit methods gave ratios of unity. The others all underestimated the 'SAR', by ca. 11%, 17% and 24% for the steady state, initial slope and decay methods, respectively.

To assess the robustness of the corrected slope and Box–Lucas methods, we then measured the magnetic heating in Ferucarbotran using selected experimental conditions to test the importance (a) of the starting temperature, T_{start}, relative to the baseline temperature, T_B and (b) of the measurement time, $t_{\max}$ (see figure 12). On inspection, it is apparent that neither method was particularly sensitive to T_{start}, as evidenced by the small standard deviations obtained over 15 separate measurements (figure 12(a)), but that the Box–Lucas method was sensitive to variations in $t_{\max}$ (figure 12(b)). This may indicate that longer measurement times are preferable for the

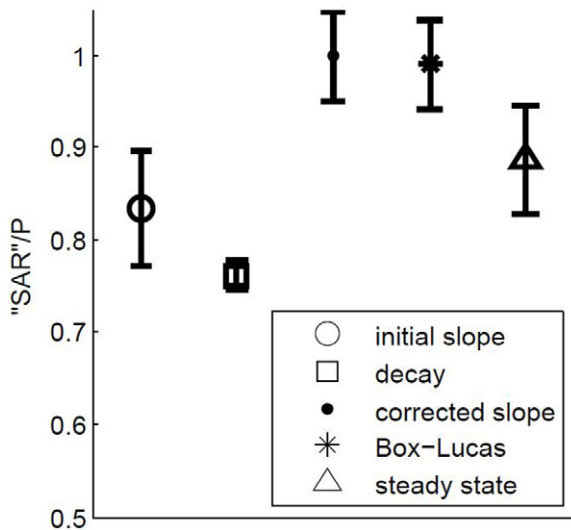J. Phys. D: Appl. Phys. **47** (2014) 495003

R R Wildeboer *et al*

Figure 11. Results of a methodological experiment in which a resistor was used to dissipate a known amount of energy, at P = 0.45 W, into a 10 ml sample of pure water. The $\Delta(t)$ heating curve was recorded and treated as if it were a magnetic heating curve. The corresponding 'SAR' values were computed using the methods described in the text, *viz.* the initial slope method ($\bigcirc$), the decay method ($\square$), the corrected slope method ($\bullet$), the Box–Lucas method ($\ast$) and the steady state method ($\triangle$). Error bars represent the standard deviation in the values obtained from five separate measurements.

Box–Lucas method so that the heating curve can saturate fully and be more easily fitted.

It is also noticeable in figure 12(*a*) that the Box–Lucas ILP value is ca. 8% lower than the corrected slope ILP value. A similar trend, albeit not so pronounced, was evident in the calibration data in figure 11. This may be an indication that in absolute terms the corrected slope method is the more accurate of the two.

To test this hypothesis, heating data were recorded on a 0.5 ml sample of 20 mg ml^{-1} FluidMag-UC/A. This is a commercially available ferrofluid whose ILP has been previously measured in adiabatic systems. In one reported experiment, conducted in an AMF of amplitude $H = 2.0$ kA m^{-1} and frequency $f = 109$ kHz, the ILP was 1.65 ± 0.03 nHm^2 kg^{-1} [15]. A similar figure was obtained in a second adiabatic experiment using $H = 1.1$ kA m^{-1} and $f = 108$ kHz, where the ILP was 1.66 ± 0.07 nHm^2 kg^{-1} [17]. In our measurement, we found an ILP of 1.68 ± 0.03 nHm^2 kg^{-1} at $H = 3.7$ kA m^{-1} and $f = 988$ kHz, for the sample mounted in an Eppendorf tube and 1.68 ± 0.08 nHm^2 kg^{-1} when the sample was mounted in a flat-bottomed glass vial. Both values are well within experimental error of the adiabatic values, hence we conclude that the corrected slope method is indeed the most accurate and reliable method of determining SAR/ILP in a non-adiabatic system.

It is interesting to reflect on the implications of this conclusion with regard to the many previously published values of SAR and ILP in magnetic hyperthermia materials. We have conducted a survey of a representative set of 50 datasets retrieved from published plots of $\Delta T(t)$ curves [18, 21, 24, 25, 30, 31, 33–38, 41, 55, 57, 58, 60, 67, 69–75]. All but three
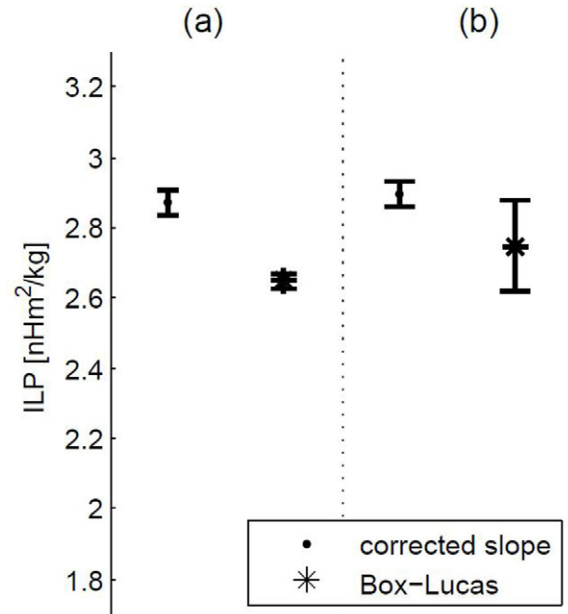

Figure 12. ILP values for a 0.5 ml 28 mg ml^{-1} Ferucarbotran sample, determined by the corrected slope ($\bullet$) and Box–Lucas ($\ast$) methods. The values are the averages obtained by analysing fifteen different heating curves: (*a*) where each curve was recorded for $t_{max} = 30$ min and the starting temperature $T_{start} = T_B$, $T_B + 2$°C and $T_B + 5$ °C relative to the baseline temperature T_B; and (*b*) where the curves were measured for $t_{max} = 5$, 16 and 30 min and $T_{start} = T_B$.

Figure 13. Representative comparison between the reported SAR values for 50 published $\Delta(t)$ curves and those calculated using the corrected slope method.

datasets had been analysed using the initial slope method, albeit using a variety of different linear approximations of the type surveyed in section 6.1, leading to both over- and underestimations of the slope. Figure 13 shows the ratio between the reported SAR value and the corrected slope value (calculated using the method described in section 6.3) for each of the fifty curves.

J. Phys. D: Appl. Phys. 47 (2014) 495003

R R Wildeboer et al

Naturally, the measurement time differed from one dataset to the next, but in every case as much of the curve as possible was used for the corrected slope calculation. If the measurement time allowed it, the slope was computed every 15 s over an interval of 60 s. (For a 5 min heating curve this resulted in 17 corrected slope values, computed over the intervals 0–60s, 15–75s, 30–90s, … 240–300s, respectively.) Furthermore, in some cases, where the complete data were not reported, assumptions had to be made regarding the baseline temperatures of the measurement systems used and the heat capacities of the samples measured. However, our calculations show these assumptions to be of relatively minor significance, affecting the derived SAR values by a few percent at most. As shown in figure 13, the variability was much more pronounced than that, with only 24% of the reported values falling within 5% of the corrected slope value.

Given that these are errors associated with the analytical process only and that in many reports little or no attention is paid to experimental errors regarding probe positioning, peripheral heating and the delayed heating effect, the total variation between reported and actual SAR/ILP values is likely to be much more.

8. Conclusions

The experimental conditions under which reliable measurements of both the SAR and ILP parameters of magnetic hyperthermia materials may be performed in a non-adiabatic system have been comprehensively reviewed and quantified. These conditions are listed in appendix 1 in the form of a set of recommendations that we hope will be applicable in most laboratories and will enable others to avoid the pitfalls that could otherwise make the measurements unreliable.

Similarly, the analytical methods by which the SAR and ILP values are extracted from the heating curves have been reviewed and tested against robust standards. We find that the most commonly used 'initial slope' method is sensitive to the experimental conditions and prone to underestimation by up to 25%. A better approximation is the full-curve fit of the 'Box–Lucas' method, although even here underestimation by up to 10% can be expected. We find that the 'corrected slope' method provides the most accurate results under the greatest range of experimental conditions and we therefore recommend that it be adopted as a standard method for SAR and ILP measurements. To assist this, details of the implementation of the corrected slope method are given in appendix 1. In addition, a simple-to-use computer program, written as an executable file in two commonly used formats (Microsoft Excel and MATLAB), is available online for free download and use [76].

Given the importance placed on the SAR and ILP parameters as determinants of good and bad materials for magnetic hyperthermia, we believe that it is essential that the experimental methods used should be scrutinised and standardised. Furthermore, given the clinical safety imperative that all materials that may be destined for medical use must be fully characterised and quantitatively analysed, it is incumbent on the hyperthermia research community to address the issue. It is in

this context that we hope that this paper will be received as a useful contribution to the field.

Appendix 1: Recommended experimental and analysis methods for SAR and ILP measurements using a non-adiabatic system.

To perform SAR and ILP measurements in a non-adiabatic system, the protocol summarized in table A1 is recommended.

It is especially important to identify the linear loss regime for any given measurement system. This is a characteristic not just of the experiment apparatus, but also of the sample surface area and volume. To do this, one should heat an MNP suspension to $\Delta T \approx 60\,°C$ above room temperature, switch off the AMF and then measure the cooling curve as the sample's temperature drops back to room temperature. The numerical derivative of the cooling curve, plotted against ΔT, should resemble figure 3. The maximum ΔT beyond which the curve is no longer linear represents the extent of the linear loss regime and no measurements should be performed beyond that value.

After calibration, one has to choose the magnetic field, frequency and particle concentration so that the heating curve will not reach temperatures that exceed the regime in which the assumption of linear losses holds. As a rule of thumb, one can estimate this by using the following criterion:

$$P = \text{SAR}_e \cdot m = \text{ILP}_e \cdot fH^2\, m < L\Delta T_{\text{lim}}, \qquad (A1)$$

in which ILP_e is the expected ILP ($\text{Hm}^2\text{kg}^{-1}$), f is the frequency (Hz), H is the magnetic field strength (A m^{-1}), m is the total particle mass (kg), L is the linear loss parameter (W K^{-1}) and ΔT_{lim} is the upper limit of the linear temperature regime (K above baseline). Both L and ΔT_{lim} may be deduced from a figure 3 style cooling curve.

Since peripheral heating can affect the natural baseline temperature for measurements, one should ensure that the heating curve starts at the temperature a water sample (of the same volume as the ferrofluid being measured) would have when a magnetic field is applied. This can be done by heating the ferrofluid for a few seconds and letting it reach a steady state before the actual measurement. For the SAR/ILP measurement itself, recording the heating curve for 5 to 10 min is usually sufficient. It does not matter whether a steady temperature state is reached during the measurement period.

With the data recorded, the SAR (and ILP) can then be calculated using the corrected slope method. We recommend that the parameter be calculated over an interval of 30–60s, at N intervals along the heating curve. This allows one to compute both the SAR/ILP parameter and the linear-loss parameter L. The following formula describes the mathematical operation of the corrected slope method:

$$\text{SAR} = \frac{1}{N} \sum_{i}^{N} \frac{C\left(\frac{dT}{dt}\right)_i + L(\Delta T)_i}{m}, \qquad (A2)$$

in which C is the heat capacity of the sample (J K^{-1}), $(dT/dt)_i$ is the slope determined by a linear fit of the data in interval

J. Phys. D: Appl. Phys. 47 (2014) 495003

R R Wildeboer *et al*

Table A1. Recommended procedure for non-adiabatic measurements of SAR and ILP.

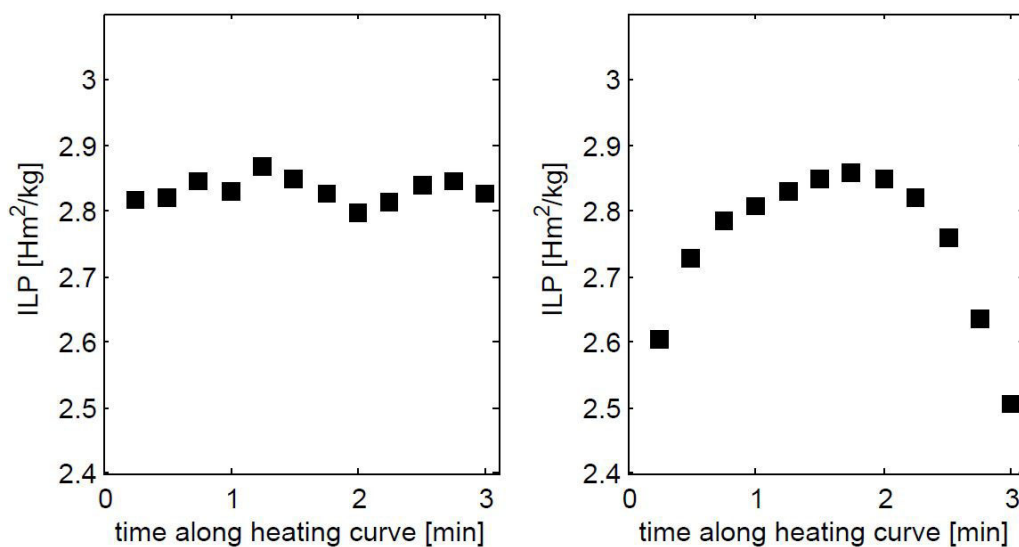|		
1.	Define the linear-loss regime	This is system-dependent, and also affected by the sample volume and container shape. It is found by recording the cooling curve after heating a MNP sample to ca. 60 °C above room temperature. Plotting the numerical derivative dT/dt versus ΔT, as in figure 3, allows one to identify the linear-loss regime. All subsequent measurements should fall within this range.
2.	Choose the measurement parameters	Use **equation A1** to choose the field amplitude, frequency and MNP concentration so that the temperature will stay within the linear-loss regime. If an estimate of the ILP is not available, a trial measurement is required.
3.	Determine the baseline temperature	The baseline temperature is the equilibrium temperature of a sample, taking into account peripheral heating. It is found by applying an AMF of the chosen amplitude and frequency to a sample of the MNP solvent alone (e.g. water), without any MNPs present. Usually the baseline temperature reaches ca. 1–3 °C above room temperature within 10–20 min.
4.	Choose the probe configuration	Multiple probes are recommended, but a single probe can be used. If two probes are used, take the mean of both as the average sample temperature. For a flat-bottomed cylindrical container use one probe, placed in the middle of the sample; or two probes, one just under and one just above the middle. For a quasi-conical container such as an Eppendorf tube use one probe, placed at 1/3 of the height below the surface; or two probes, one just below the surface and one 2/3 down.
5.	Equilibrate before the measurement	Magnetically heat the sample a few degrees in order for the system to 'warm up' before the start of actual measurement. The measurement can be performed once the sample has cooled down to the baseline temperature, as defined in step 3.
6.	Perform the measurement	Record the temperature for 1 to 2 min before applying the AMF, so that the baseline temperature is noted and any time delay effects are captured. It is usually sufficient to measure the temperature once every 1 to 5 s during a AMF application of 5 to 10 min.
7.	Calculate the heating ability	Use the Matlab or Excel programme provided to calculate the heating ability (either the SAR or the ILP) using the corrected slope method. In most cases it is safe to assume a heat capacity equal to that of the MNP solvent. Making a few repeated measurements may help to estimate the experimental error.

Figure A1. ILP measurement for a Ferucarbotran sample calculated by the corrected slope method at twelve points along the heating curve: (left) for an accurate measurement within the linear-loss region and (right) for an inappropriate measurement design for which the rate and extent of heating exceeded the linear-loss regime.

i and ΔT_i is the difference between the mean temperature of interval i and the baseline temperature.

Calculating the slope at different positions on the heating curve gives one an estimate of the accuracy of the measurement and is also a useful way to check that a reliable experiment has been performed. This is illustrated in figure A1 for a 0.5 ml sample of Ferucarbotran (28 mg ml^{-1} iron), for which the ILP was calculated at 12 points in the first 3 min of the heating curve. The reliable measurement is largely flat, while the unreliable one is clearly curved.

The corrected slope fits also provide an estimate of the linear loss parameter, L. Typical values that we have measured for L have been ca. 6 mW K^{-1} for a plastic Eppendorf tube, 11 mW K^{-1} for a flat-bottomed glass vial and 9 mW K^{-1} for a flat-bottomed vial made from PLA. These values roughly follow the container material's conductance coefficient (0.25 W mK^{-1} [77], 1.1 W mK^{-1} [78] and 0.12 W mK^{-1} [54] for polypropylene, glass and PLA, respectively), but shape and wall thickness also contribute to the measured L. This underlines the need to measure L on a case-by-case basis.

J. Phys. D: Appl. Phys. 47 (2014) 495003

R R Wildeboer et al

The authors have written and made available for free download and use a corrected slope data analysis program [76]. Versions are provided in both MATLAB (Mathworks 2013b, Natick, MA) and in Excel (Microsoft Office 2007).

References

[1] Ortega D and Pankhurst Q A 2013 Magnetic hyperthermia in Nanoscience *Nanostructures through Chemistry* ed P O'Brien (Cambridge: The Royal Society of Chemistry) p 60–88

[2] Hilger I, Hergt R and Kaiser W A 2005 Use of magnetic nanoparticle heating in the treatment of breast cancer *IEEE Proc. Nanobiotechnol.* **152** 33–9

[3] Pankhurst Q A *et al* 2009 Progress in applications of magnetic nanoparticles in biomedicine *J. Phys. D: Appl. Phys.* **42** 224001

[4] Pankhurst Q A *et al* 2003 Applications of magnetic nanoparticles in biomedicine *J. Phys. D: Appl. Phys.* **36** R167–81

[5] Dutz S and Hergt R 2013 Magnetic nanoparticle heating and heat transfer on a microscale: basic principles, realities and physical limitations of hyperthermia for tumour therapy *Int. J. Hyperthermia* **29** 790–800

[6] Gilchrist R K *et al* 1957 Selective inductive heating of lymph nodes *Ann. Surg.* **146** 596–606

[7] Johannsen M *et al* 2005 Clinical hyperthermia of prostate cancer using magnetic nanoparticles: presentation of a new interstitial technique *Int. J. Hyperthermia* **21** 637–47

[8] Thiesen B and Jordan A 2008 Clinical applications of magnetic nanoparticles for hyperthermia *Int. J. Hyperthermia* **24** 467–74

[9] Online search conducted on 1 July 2014 of the Web of Science and PubMed databases, using 'magnet* and hypertherm*' as the topic search item

[10] Reilly J P 1992 Principles of nerve and heart excitation by time-varying magnetic fields *Ann. New York Acad. Sci.* **649** 96–17

[11] Atkinson W J, Brezovich I A and Chakraborty D P 1984 Usable frequencies in hyperthermia with thermal seeds *IEEE Trans. Biomed. Eng.* **BME-31** 70–5

[12] Rosensweig R E 2002 Heating magnetic fluid with alternating magnetic field *J. Magn. Magn. Mater.* **252** 370–4

[13] Kallumadil M *et al* 2009 Suitability of commercial colloids for magnetic hyperthermia *J. Magn. Magn. Mater.* **321** 1509–13

[14] Andreu I and Natividad E 2013 Accuracy of available methods for quantifying the heat power generation of nanoparticles for magnetic hyperthermia *Int. J. Hyperthermia* **29** 739–51

[15] Natividad E, Castro M and Mediano A 2009 Adiabatic versus non-adiabatic determination of specific absorption rate of ferrofluids *J. Magn. Magn. Mater.* **321** 1497–500

[16] Natividad E, Castro M and Mediano A 2011 Adiabatic magnetothermia makes possible the study of the temperature dependence of the heat dissipated by magnetic nanoparticles under alternating magnetic fields *Appl. Phys. Lett.* **98** 243119

[17] Natividad E, Castro M and Mediano A 2008 Accurate measurement of the specific absorption rate using a suitable adiabatic magneto thermal setup *Appl. Phys. Lett.* **92** 093116

[18] Yuan Y and Tasciuc D-A B 2011 Comparison between experimental and predicted specific absorption rate of functionalized iron oxide nanoparticle suspensions *J. Magn. Magn. Mater.* **323** 2463–9

[19] Incorpera F P 2007 *Fundamentals of Heat and Mass Transfer* (Danvers, MA: John Wiley and Sons)

[20] O'Sullivan C T 1990 Newton's law of cooling - a critical assessment *Am. J. Phys.* **58** 956–660

[21] Teran F J *et al* 2012 Accurate determination of the specific absorption rate in super paramagnetic nanoparticles under non-adiabatic conditions *Appl. Phys. Lett.* **101** 062413

[22] Hiergeist R *et al* 1999 Application of magnetite ferrofluids for hyperthermia *J. Magn. Magn. Mater.* **201** 420–2

[23] Box G E P and Lucas H L 1959 Design of experiments in non-linear situations *Biometrika* **46** 77–90

[24] Murase K *et al* 2013 Control of the temperature rise in magnetic hyperthermia with use of an external static magnetic field *Physica Med.* **29** 624–30

[25] Bordelon D E *et al* 2011 Magnetic nanoparticle heating efficiency reveals magneto-structural differences when characterized with wide ranging and high amplitude alternating magnetic fields *J. Appl. Phys.* **109** 124904

[26] Huang S *et al* 2012 On the measurement technique for specific absorption rate of nanoparticles in an alternating electromagnetic field *Meas. Sci. Technol.* **23** 035701

[27] Wang S-Y, Huang S and Borca-Tasciuc D 2013 Potential sources of errors in measuring and evaluating the specific loss power of magnetic nanoparticles in an alternating magnetic field *IEEE Trans. Magn.* **49** 255–62

[28] Schnelle W and Gmelin E 2002 Critical review of small sample calorimetry: improvement by auto-adaptive thermal shield control *Thermochim. Acta* **391** 41–9

[29] Lacroix L M, Carrey J and Respaud M 2008 A frequency-adjustable electromagnet for hyperthermia measurements on magnetic nanoparticles *Rev. Sci. Instrum.* **799** 093909

[30] Liu X L *et al* 2014 Magnetic nanoparticle-loaded polymer nanospheres as magnetic hyperthermia agents *J. Mater. Chem.* B **2** 120–8

[31] Rashid A U *et al* 2013 Strontium hexaferrite (SrFe12O19) based composites for hyperthermia applications *J. Magn. Magn. Mater.* **344** 134–9

[32] Skumiel A *et al* 2007 Heating effect in biocompatible magnetic fluid *Int. J. Thermophys.* **28** 1461–9

[33] Hayashi K *et al* 2008 Synthesis of spinel iron oxide nanoparticle/organic hybrid for hyperthermia *J. Mater. Res.* **23** 3415–24

[34] Nomura S *et al* 2007 Inductive heating of Mg ferrite powder in high-water content phantoms using ac magnetic field for local hyperthermia *Heat Transfer Eng.* **28** 1017–22

[35] Salloum M *et al* 2008 Controlling nanoparticle delivery in magnetic nanoparticle hyperthermia for cancer treatment: experimental study in agarose gel *Int. J. Hyperthermia* **24** 337–45

[36] Drake P *et al* 2007 Gd-doped iron-oxide nanoparticles for tumour therapy via magnetic field hyperthermia *J. Mater. Chem.* **17** 4914–8

[37] Nguyen X P *et al* 2012 Iron oxide-based conjugates for cancer theragnostics *Adv. Nat. Sci.: Nanosci. Nanotechnol.* **3** 033001

[38] Aono H *et al* 2012 High heat generation ability in ac magnetic field for nano-sized magnetic Y3Fe5O12 powder prepared by bead milling *J. Magn. Magn. Mater.* **324** 1985–91

[39] Motoyama J *et al* 2008 Size dependent heat generation of magnetite nanoparticles under ac magnetic field for cancer therapy *BioMagn. Res. Technol.* **6** 4

[40] Bordelon D E *et al* 2012 Modified solenoid coil that efficiently produces high amplitude ac magnetic fields with enhanced uniformity for biomedical applications *IEEE Trans. Magn.* **48** 47–52

[41] Kasuya R *et al* 2010 Heat dissipation characteristics of magnetite nanoparticles and their application to macrophage cells *Phys. Proc.* **9** 186–9

[42] Ahrentorp F *et al* 2010 Sensitive high frequency ac susceptometry in magnetic nanoparticle applications *AIP Conf. Proc.* **1311** 213–23

J. Phys. D: Appl. Phys. **47** (2014) 495003

R R Wildeboer *et al*

[43] Cano M E *et al* 2011 An induction heater device for studies of magnetic hyperthermia and specific absorption ratio measurements *Rev. Sci. Instrum.* **82** 114904

[44] Goya G F, Grazu V and Ibarra M R 2008 Magnetic nanoparticles for cancer therapy *Curr. Nanosci.* **4** 1–16

[45] Jordan A *et al* 2009 Inductive heating of ferrimagnetic particles and magnetic fluids: physical evaluation of their potential for hyperthermia *Int. J. Hyperthermia* **25** 499–11

[46] Laurent S *et al* 2011 Magnetic fluid hyperthermia: focus on superparamagnetic iron oxide nanoparticles *Adv. Colloid Interface Sci.* **166** 8–23

[47] Miyata R *et al* 2005 Temperature distributions of developed needle type applicator in *27th Annual Int. Conf. Engineering in Medicine and Biology Society IEEE-EMBS* (*Shanghai*) p 6801–4

[48] Mornet S *et al* 2006 Magnetic nanoparticle design for medical applications *Prog. Solid State Chem.* **34** 237–47

[49] Ma M *et al* 2004 Size dependence of specific power absorption of Fe3O4 particles in ac magnetic field *J. Magn. Magn. Mater.* **268** 33–9

[50] Ishihara Y *et al* 2013 Evaluation of magnetic nanoparticle samples made from biocompatible ferucarbotran by time-correlation magnetic particle imaging reconstruction method *BMC Med. Imaging* **13** 1–10

[51] Reimer P and Balzer T 2003 Ferucarbotran (Resovist): a new clinically approved RES-specific contrast agent for contrast-enhanced MRI of the liver: properties, clinical development, and applications *Eur. Radiol.* **13** 1266–76

[52] Araya T *et al* 2013 Antitumor effects of inductive hyperthermia using magnetic ferucarbotran nanoparticles on human lung cancer xenografts in nude mice *Onco Targets Ther.* **6** 237–42

[53] Takamatsu S *et al* 2008 Selective induction hyperthermia following transcatheter arterial embolization with a mixture of nano-sized magnetic particles (ferucarbotran) and embolic materials: feasibility study in rabbits *Radiat. Med.* **26** 179–87

[54] Lim L T, Auras R and Rubino M 2008 Processing technologies for poly(lactic acid) *Prog. Polym. Sci.* **33** 820–52

[55] Patil R M *et al* 2014 Non-aqueous to aqueous phase transfer of oleic acid coated iron oxide nanoparticles for hyperthermia application *RSC Adv.* **4** 4515–22

[56] Suto M *et al* 2009 Heat dissipation mechanism of magnetite nanoparticles in magnetic fluid hyperthermia *J. Magn. Magn. Mater.* **321** 1493–6

[57] Kobayashi H *et al* 2011 Self-heating property of magnetite nanoparticles dispersed in solution *IEEE Trans. Magn.* **47** 4151–4

[58] Sharma M S Mantri and Bahadur D 2012 Study of carbon encapsulated iron oxide/iron carbide nanocomposite for hyperthermia *J. Magn. Magn. Mater.* **324** 3975–80

[59] Hilger I *et al* 2002 Heating potential of iron oxides for therapeutic purposes in interventional radiology *Acad. Radiol.* **9** 198–202

[60] Lartigue L *et al* 2012 Cooperative organization in iron oxide multi-core nanoparticles potentiates their efficiency as heating mediators and MRI contrast agents *ACS Nano* **6** 10935–49

[61] Shokuhfar A and Seyyed Afghahi S 2013 The heating effect of iron-cobalt magnetic nanofluids in an alternating magnetic field: application in magnetic hyperthermia treatment *Nanoscale Res. Lett.* **8** 1–11

[62] Kline T L *et al* 2009 Biocompatible high-moment FeCo-Au magnetic nanoparticles for magnetic hyperthermia treatment optimization *J. Magn. Magn. Mater.* **321** 1525–8

[63] Mehdaoui B *et al* 2011 Optimal size of nanoparticles for magnetic hyperthermia: a combined theoretical and experimental study *Adv. Funct. Mater.* **21** 4573–81

[64] Shah S A, Hashmi M U and Alam S 2011 Effect of aligning magnetic field on the magnetic and calorimetric properties of ferrimagnetic bioactive glass ceramics for the hyperthermia treatment of cancer *Mater. Sci. Eng.:* C **31** 1010–6

[65] Tai C-C and Chen C-C 2008 The Design of a half-bridge series-resonant type heating system for magnetic nanoparticle thermotherapy *PIERS Online* **4** 276–80

[66] Lima E Jr *et al* 2013 Size dependence of the magnetic relaxation and specific power absorption in iron oxide nanoparticles *J. Nanopart. Res.* **15** 1654

[67] Marcos-Campos I *et al* 2011 Cell death induced by the application of alternating magnetic fields to nanoparticle-loaded dendritic cells *Nanotechnology* **22** 205101

[68] Le Renard P-E *et al* 2011 Magnetic and *in vitro* heating properties of implants formed *in situ* from injectable formulations and containing super paramagnetic iron oxide nanoparticles (SPIONs) embedded in silica microparticles for magnetically induced local hyperthermia *J. Magn. Magn. Mater.* **323** 1054–63

[69] Timko M *et al* 2009 Magnetic properties and heating effect in bacterial magnetic nanoparticles *J. Magn. Magn. Mater.* **321** 1521–4

[70] Xu R *et al* 2007 Measurement of specific absorption rate and thermal simulation for arterial embolization hyperthermia in the maghemite–gelled model *IEEE Trans. Magn.* **43** 1078–85

[71] Thomas L A 2010 *Nanoparticle Synthesis For Magnetic Hyperthermia, in Chemistry* (London: University College London)

[72] Thorat N D *et al* 2013 Surface functionalized LSMO nanoparticles with improved colloidal stability for hyperthermia applications *J. Phys. D: Appl. Phys.* **46** 105003

[73] Khot V M *et al* 2013 Induction heating studies of dextran coated MgFe2O4 nanoparticles for magnetic hyperthermia *Dalton Trans.* **42** 1249–58

[74] Do H M *et al* 2011 Magnetic heating characteristics of La 0.7 Sr x Ca 0.3– x MnO 3 nanoparticles fabricated by a high energy mechanical milling method *Adv. Nat. Sci.: Nanosci. Nanotechnol.* **2** 035003

[75] Tran D L *et al* 2010 Biomedical and environmental applications of magnetic nanoparticles *Adv. Nat. Sci.: Nanosci. Nanotechnol.* **1** 045013

[76] Corrected-slope SAR and ILP analysis programmes, written in Microsoft Excel and MatLab formats (www. resonantcircuits.com)

[77] Weidenfeller B, Höfer M and Schilling F R 2004 Thermal conductivity, thermal diffusivity, and specific heat capacity of particle filled polypropylene *Compos. Part A: Appl. Sci. Manuf.* **35** 423–9

[78] Lagally E T and Mathies R A 2004 Integrated genetic analysis microsystems *J. Phys. D: Appl. Phys.* **37** R245–61